Journal of Manufacturing Systems 56 (2020) 587–597

Contents lists available at ScienceDirect

Journal of Manufacturing Systems

journal homepage: www.elsevier.com/locate/jmansys

Efficiently registering scan point clouds of 3D printed parts for shape accuracy assessment and modeling

Nathan Decker*, Yuanxiang Wang, Qiang Huang

Department of Industrial and Systems Engineering, University of Southern California 3715 McClintock Ave, GER 240, Los Angeles, CA, 90089-0193, United States

ARTICLE INFO

Keywords:
Iterative closest point (ICP)
Registration
Additive manufacturing (AM)
3D printing (3DP)
Dimensional accuracy assessment
Geometric deviations

ABSTRACT

One popular approach to assess the geometric differences between a part produced by additive manufacturing (AM) and its intended design is the use of a 3D scanner to produce a point cloud. This digital scan is then aligned against the part's intended design, allowing for quantification of print accuracy. One of the most common methods for achieving this alignment is the Iterative Closest Point (ICP) algorithm. This paper evaluates several potential pitfalls that can be encountered when applying ICP for assessment of dimensional accuracy of AM parts. These challenges are then illustrated using simulated data, allowing for quantification of their impact on the accuracy of deviation measurements. Each of these registration errors was shown to be significant enough to noticeably affect the measured deviations. An efficient and practical method to address several of these errors based on engineering informed assumptions is then presented. Both the proposed method and traditional unconstrained ICP are used to produce alignments of real and simulated measurement data. A real designed experiment was conducted to compare the results obtained by the two registration methods using a linear mixed effects modeling approach. The proposed method is shown to produce alignments that were less sensitive to variation sources, and to generate deviation measurements that will not underestimate the true shape deviations as the unconstrained ICP algorithm commonly does.

1. Introduction

One major challenge in the field of additive manufacturing (AM) is to ensure the accuracy of produced parts, which can often deviate significantly from the intended design. Substantial work has been done in the literature to provide strategies to control these deviations. These efforts fall into a number of broad categories, including process parameter optimization [1–7], product design adjustment [8–12], and online monitoring [13–18]. One unifying task that must be completed as a prerequisite for performing or assessing the efficacy of each of these approaches is the assessment of part accuracy.

1.1. Accuracy assessment using scanned point clouds

There are many ways to measure the accuracy of a manufactured part. These can range in complexity and cost from measurement of predefined dimensions using calipers to the use of a CT scanner for whole surface measurement [19–22]. To fully assess and control quality of parts produced by AM, it is necessary to know the magnitude and direction of deviation across the entire surface of a part. One method that is growing in popularity is the use of a 3D scanner to generate a digital cloud of points that replicate the object being scanned. These 3D scanners utilize a range of technologies for surface reconstruction, including structured light scanning, laser triangulation, and photogrammetry [23–27]. Once a point cloud of the manufactured object is generated, it must be aligned (or registered) against a reference computer aided design (CAD) or other 3D model representing the object's ideal shape and size [28]. After this is completed, deviations between the two surfaces can be calculated.

This alignment can be produced using a number of algorithms that have been developed in the past few decades. Several of the most common algorithms are described in detail below, though the list is certainly not exhaustive. A more comprehensive discussion of the topic of registration can be found in Tam et al. [29].

1.2. Background and literature review

One simple and commonly utilized alignment method is point pairs picking [30]. With this method, a user is first asked to pick several pairs of corresponding points on both the scanned point cloud, and the shape that it will be aligned to. These should be located across the surface of the object. Then, the transformation (translation/rotation) of the scan

* Corresponding author.
E-mail address: ndecker@usc.edu (N. Decker).

https://doi.org/10.1016/j.jmsy.2020.04.001
Received 3 April 2020; Accepted 3 April 2020
Available online 21 April 2020

point cloud that minimizes the sum of the distances between these pairs of points is calculated and applied. In the case of rigid registration (where both shapes are identical), this transformation can be perfectly determined with just three point pairs [31]. In situations where deviation between the two shapes is to be measured, such as AM accuracy assessment, more points are needed to achieve a quality alignment. Smith, et al. [32], for example, utilized eight landmark points across the surface to perform alignment of scan point clouds of 3D printed parts produced on an FDM printer with their corresponding CAD file.

Another common method for achieving alignment is the 4PCS Algorithm [31]. This algorithm is designed to produce alignment in cases where point sets include outliers and noise. Further, the algorithm can be successfully applied without any prefiltering or initial alignment [31]. It functions by finding coplanar 4-points bases in the first point cloud that also correspond to 4-points bases in the second point cloud. A base is set of points that have good candidate correspondences between the two point clouds. Using these corresponding bases, the optimal transformation to align the two point clouds is determined [33]. A number of variants and modifications to this algorithm can be found in the literature [34,35].

Finally, one of the most frequently used tools for alignment is the iterative closest point (ICP) algorithm developed by Besl and McKay [36]. This algorithm is capable of aligning geometric representations including point sets, line segment sets, implicit curves, parametric curves, triangle sets, implicit surfaces, and parametric surfaces [36]. For the two point clouds to be aligned, the first point cloud is called the "data" shape, which is produced using a 3D scanner in this application. The second is the "model" shape, which represents the ideal for shape and position. The ICP algorithm consists of the following set of steps:

1 For each point on the data shape, determine the closest corresponding point on the model shape.
2 Find the transformation (translation/rotation) of the data shape that minimizes the mean of the squares of distances between these point pairs.
3 Apply the transformation to the data shape.
4 Calculate the mean square distance for the point pairs. If the difference between this mean square distance and the previous one is below a preset threshold, stop. Otherwise, repeat from Step 1.

The final alignment of the data shape is then outputted as the resulting transformation.

A large number of works have utilized ICP to align scan point clouds of manufactured parts against their CAD designs for the purpose of deviation calculation. In the AM literature, Klar, et al. [37] measured the dimensional accuracy of 3D printed rectangular prisms of high consistency nanocellulose. They began by fitting planes to each face of a prism's scan point cloud. The mean distance between each of these planes was then used to generate a new 'ideal' rectangular prism. This new rectangular prism was first aligned to the scan point cloud by eye, and then secondly aligned to the point cloud using the ICP algorithm implemented in CloudCompare, an open source program for working with point clouds and triangular meshes [38]. Following this alignment, the distances to the new prism shape were calculated for each point on the scan point cloud.

Alharbi, et al. [39] studied the dimensional accuracy of 3D printed dental restorations produced using stereolithography. Scans of their printed parts were aligned to the STL file that they were printed from, which represents the ideal shape of the printed part. The first alignment step was done by eye, followed by ICP. Finally, the distances between the STL file and printed parts were calculated.

Because the shape of a 3D printed part being evaluated will differ slightly from the design it is being registered against, this is an instance of nonrigid registration. Unfortunately, nonrigid registration tends to be a more difficult challenge than rigid registration [29]. Further, alignments that are produced by the ICP algorithm can differ as a result of factors such as scan density, completeness of the scan, differing initial alignments, and convergence to differing local minimums. In order to meet these challenges, a number of improvements to the ICP algorithm have been proposed.

ICP variants using resampling have been proposed as a means of avoiding convergence to poor alignments. Gelfand, et al. [40] proposed modifications to the ICP algorithm that sampled points on regions of the aligned shapes that had geometries considered to be more 'stable'. These geometries are complex, and only allow translation or rotation with changes in the algorithm's error metric. Kwok and Tang [41] used stability analysis to improve upon normal space sampling, resulting in a more efficient and robust registration algorithm. Yu, et al. [42] proposed a method that resamples and removes noise from points on the point clouds to be aligned, increasing accuracy when the algorithm is applied to 3D face verification.

Chetverikov et al. [43,44] proposed the addition of trimming to the ICP algorithm to allow ICP to accurately converge in the presence of substantial differences between the data and model shapes. In this formulation, Least Trimmed Squares is used as the error metric to be minimized in Step 2 of the ICP algorithm. As a result of this, the presence of outliers and deviations in the shapes to be aligned has less of an impact on the final alignment, as the largest point to point distances are ignored. Dong et al. [45] built on this approach by adding Lie group representations to determine geometric transformations when anisotropic scaling is also desired.

Minguez, et al. [46] and Armesto et al. [47] proposed the Metric-Based ICP Technique as a means of improving the algorithm's robustness and precision. This method replaces Euclidean distance with a new distance measure that takes into account both translation and rotation, both of which are relevant to proper alignment.

Kapoutsis, et al. [48,49] proposed the Morphological ICP algorithm, which reduces the computational complexity of ICP's closest corresponding point operator. This method starts by building a Voronoi diagram of model points using the morphological Voronoi tessellation method. Then closest corresponding points can be determined using the diagram. This reduces the computational cost of the operation from $O(N_pN_x)$ to $O(N_p)$ where N_p and N_x are the number of points in the data shape and model shape respectively.

Finally, because convergence to a global minimum is highly desirable for ensuring that the ICP algorithm doesn't converge to an unreasonable local minimum, Yang, et al. [50] proposed Go-ICP, which uses the branch and bound method to search SE(3) space for a transformation that reduces the distance objective function value. ICP is then performed with this initialized position, and the result is set as the upper bound for the next branch and bound search. This process is repeated until convergence to a desired accuracy.

While each of these proposed methods offers strong gains over the conventional ICP algorithm, their use for applications in AM faces a significant challenge. Namely, the alignment that minimizes deviations between two surfaces isn't necessarily the most reasonable alignment for applications that seek to model and correct deviations of printed parts. Instead, it is desirable that the algorithm for aligning surfaces takes into account pre-existing knowledge of the manufacturing process and produces alignments that make sense in light of this information. This point will be elaborated on in Section 2.2. As a result, a registration methodology that addresses the challenges posed by ICP while also incorporating manufacturing process knowledge is needed.

1.3. Scope and contributions

The first contribution of this paper is to identify some of the challenges posed by ICP when applied to assessing the accuracy of AM built parts. This discussion is necessary because ICP is one of the most frequently used tools for 3D scan point cloud alignment in the AM literature. It is important to note here that while ICP wasn't proposed with manufacturing quality assessment in mind, it has become popular in

this context. A number of these potential pitfalls will be discussed in depth in Section 2 and quantitatively evaluated using simulated data in Section 4. Other discussions of these pitfalls are available in the literature, however, this study seeks to uniquely make the issue evident in the context of AM. While other algorithms differ in how alignment is achieved, many of the points that will be covered in this paper will potentially apply to them to a varying extent.

Second, a systematic approach to registration of point clouds specifically for AM quality assessment will be presented in Section 3. This approach is designed to minimize variability and inaccuracies from ICP alignment, while keeping deviations from a part's design as close to where they originated as possible. This is done through the use of geometric constraints on the ICP algorithm's alignment based on manufacturing process knowledge. The methodology utilizes the ICP algorithm, but does not fundamentally alter it. Finally, a quantitative case study will be conducted in order to assess the potential magnitude of deviations in ICP point cloud alignments before and after the application of the proposed registration methodology. This will also be described in Section 4.

2. Types of registration errors

Because of the potential biases introduced by the ICP algorithm, as well as the inherent challenges of non-rigid registration, the deviation measurements produced after registration of scan point clouds are not always indicative of a 3D printed part's error. This section will examine a number of potential pitfalls. These alignment errors can be due to a number of factors including selective scanning, error minimization bias, and convergence to a local minimum that is far from the global minimum.

2.1. Non-uniform sampling/scanning

The first category of errors that will be illustrated here is selective scanning induced errors. Many factors, such as a surface's reflectivity or angle with respect to a scanner can impact the density of a scan point cloud. Further, someone manually scanning a part using a laser scanner, for instance, might conduct multiple passes of a certain region but only one of another region. This would result in a point cloud of varying density. It is also possible that certain surfaces on the shape might be inaccessible to the scanner, meaning that they remain unscanned. One example of this would be a deep recess in a part. Finally, when a part is scanned while resting on a worktop or other surface, the bottom of the part will often remain unscanned, since this region of the scan will be inaccessible to the 3D scanner unless multiple scans are performed. This results in a point cloud of just the top surfaces of a shape. This inconsistency in the density of a scan point cloud can greatly impact the alignment produced by the ICP algorithm.

Because the ICP algorithm seeks to minimize the mean of the squares of distances between the closest point pairs, registration will be biased towards alignments that minimize deviation in regions with greater point cloud density [36]. As a consequence, regions with lower point cloud density will be aligned with greater deviation. This effect is illustrated in 2D in Fig. 1. The top diagram shows how a scanned part with uniform lateral shrinkage would intuitively be registered against its CAD design. The bottom diagram roughly illustrates the effect of the differing point cloud density on final alignment.

2.2. Deviation minimization bias due to unconstrained registration

A similar issue occurs when a scan only contains points from the top surface of an object. This is often done out of necessity, since it is difficult to position a part in order to allow its entire surface to be scanned. In this instance, the ICP algorithm will work to minimize the deviation found on the top surface of the part, without the bottom surface acting as a constraint on the alignment. Consequently, the top surface will be pulled into near alignment with the reference part, irrespective of where the bottom of the scanned part would naturally be found. This can result in a substantial underestimation of dimensional inaccuracy. This situation is illustrated in Fig. 2. The top diagram shows a natural alignment of a part with inadequate height against its CAD design. It should be noted here that what constitutes a natural alignment between a deformed part and its CAD design depends on the assumptions that are made. In this case, it will be assumed that the bottom surface of a printed part is manufactured with perfect accuracy. This assumption will be explained further in Section 3. It can be seen that under this alignment, there is substantial geometric deviation between the two shapes.

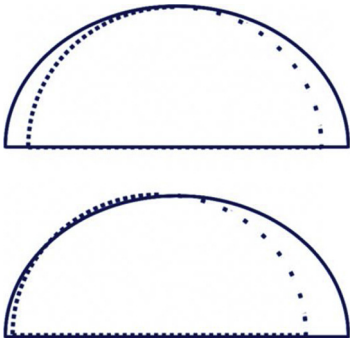

Fig. 1. (Top) CAD design and point cloud of part with lateral shrinkage (Bottom) Alignment of point cloud with inconsistent density after ICP.

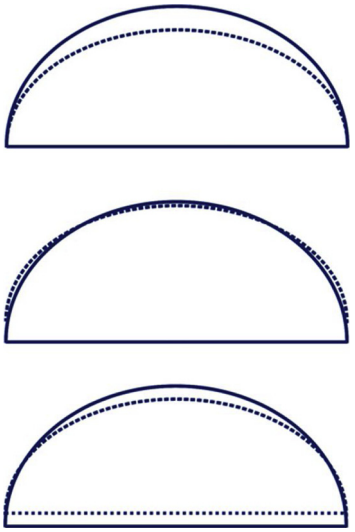

Fig. 2. (Top) CAD design and point cloud of part with vertical shrinkage (Middle) Alignment of point cloud without bottom points after ICP (Bottom) Alignment of point cloud with bottom points after ICP.

The difference in alignments produced for shapes with and without bottom points is illustrated in the middle and bottom diagrams. Interestingly, even with bottom points, ICP aligns the point cloud in the center of the intended design. These two examples highlight a significant tendency of the ICP algorithm: to spread overall shape deviation. In the context of aligning two similar shapes, this makes sense, however in the context of finding dimensional deviations in 3D printed parts, this is problematic. The alignment that minimizes the mean of the squares of distances between closest point pairs might not adequately represent a printer's build errors. If a printed part only deviates from its design in a specific area, for instance, this error can be spread across the whole shape. This can make there appear to be less error than there actually is, and remove deviations from the region in which they were produced. In the bottom diagram of Fig. 2, for instance, while the

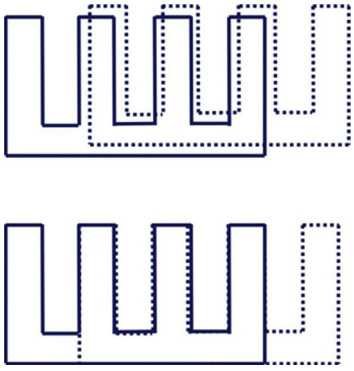

Fig. 3. (Top) CAD design and point cloud of part with no errors. (Bottom) Alignment of point cloud after ICP.

bottom surface of the dome was printed without any deviation, it will show deviation. Conversely, the top surface will show less deviation from its design than is actually present.

These pitfalls occur because the ICP algorithm isn't constrained by the realities of the manufacturing process that was used to produce the part being evaluated. Engineering informed assumptions derived from how the part was created help a user to determine what alignments make sense in light of prior knowledge. Unconstrained ICP doesn't benefit from this knowledge.

2.3. Local minimum errors

The ICP algorithm has been proven to always converge monotonically to a local minimum solution as defined by the mean-square distance function [36]. One issue with this is that the most logical alignment of a point cloud may not be the local minimum that the ICP algorithm converges to. In the context of scanned point clouds of 3D printed parts, the globally optimal solution may not be the most logical alignment either, as was discussed in the previous section. An extreme example of this issue is illustrated in Fig. 3. Here, the algorithm gets trapped in a local minimum that is clearly not a reasonable alignment of the two point clouds. Subtle versions of this can prove to be more problematic.

3. Error reduction strategy

In order to address some of these potential pitfalls, a methodology for producing repeatable and reasonable alignments in the context of additive manufacturing quality control using the ICP algorithm is presented here. To address issues due to non-uniform scan density, uniform resampling of a scan point cloud is performed. The method also uses engineering-informed assumptions about the 3D printing process to constrain the ICP algorithm and limit deviation minimization bias. Finally, a strong initial alignment is produced before ICP is utilized, increasing the likelihood ICP converges to a reasonable minimum. We have briefly presented an earlier version of this methodology in [51]. Improvements in this version include the ability to account for non-uniform scanning/sampling, as well as guidance for mitigating issues caused by convergence to unreasonable local minima. An overview of the method is given by the flowchart in Fig. 4.

3.1. Initial positioning of scan point cloud

It is necessary to first align the scanned point cloud by eye as closely with the reference CAD surface as possible. This helps to prevent the more egregious variety of local minimum errors discussed in Section 2.3. Methods such as the one presented in [30] might be utilized to simplify this process.

3.2. Scan point cloud segmentation

It will be assumed that the part was resting on a flat worktop during scanning. The second step in this procedure is separating the scan point cloud into two sets: table points Q_{table} and shape points Q_{shape}. Table points are generated when the scanner scans the surface the object is resting on. This is illustrated in Fig. 5. This separation can be achieved using an automated algorithm, such as the one presented in [52] and implemented in CloudCompare.

3.3. Reorientation of scan point cloud

Once the scanned point cloud is segmented, it is necessary to perform an initial alignment with respect to the ideal reference shape. This is done using an engineering informed assumption. For many extrusion, vat-polymerization, selective sintering, and directed energy deposition-based 3D printing processes, material is applied to a roughly perfectly flat build plate to form the bottom of an additively manufactured part. In this case, it becomes reasonable to assume that the bottom of a 3D printed part is produced with perfect accuracy. For some AM processes, this assumption might not be reasonable. One example of this is a part built in the middle of a powder bed fusion build chamber. It should also be noted that in the presence of warping, this assumption would no longer be valid. While this requirement is a strong one, it should be noted that with care, it can be applied to many situations. This is because the aforementioned compatible AM methods make up the vast majority of the AM market share. If this assumption is reasonable, then the print errors on the object can be attributed to the rest of the object's surface. This implies that the planes representing the bottom of the scanned point cloud and the bottom of the reference CAD shape should be parallel and intersecting.

This can be implemented according to the following procedure. If a plane $f(x,y,z) = \beta_1 x + \beta_2 y + \beta_3 z + \beta_0 = 0$ is fit to the table points Q_{table}, then the vector $\mathbf{N_{Scan}} = \nabla f = [\beta_1 \ \beta_2 \ \beta_3]^T$, points in the direction normal to the bottom surface of the scanned point cloud. $\mathbf{N_{Scan}}$ should be made equal to $\mathbf{N_{CAD}}$, which in most cases will be: $[0 \ 0 \ -1]^T$. This is illustrated in Fig. 6.

Once the bottom of the scan point cloud is made parallel to the bottom of the CAD reference shape, it is necessary to remove any distance between the two parallel planes. In the case that the bottom of CAD reference shape falls on the x-y plane, β_0 of plane f should be set to zero, leading in a translation along the z-axis. Once this final alignment is achieved, the table points can be disregarded. Translation and rotation of the scan point cloud can be achieved using affine transformation matrices. One computationally inexpensive algorithm for aligning two vectors is presented by Möller and Hughes [53], and can be utilized for this purpose.

3.4. Point cloud resampling with SPSR to achieve uniform point cloud density

In the event that the scan point cloud is unevenly dense, sparse, or contains many unreasonable outliers, it is possible to generate a more consistent point cloud using Screened Poisson Surface Reconstruction (SPSR). This algorithm is explained in [54] and implemented in many open source applications. The first step of this process is to generate a mesh from the point cloud using SPSR. Then a large number of points can be randomly sampled from this mesh, resulting in a more uniform scan point cloud. One tradeoff of this approach is the potential smoothing of fine features. It is important to monitor this, and adjust parameters accordingly. SPSR is illustrated in Fig. 7 and 8 .

3.5. ICP implementation

At this point, fine-resolution registration can be obtained using the

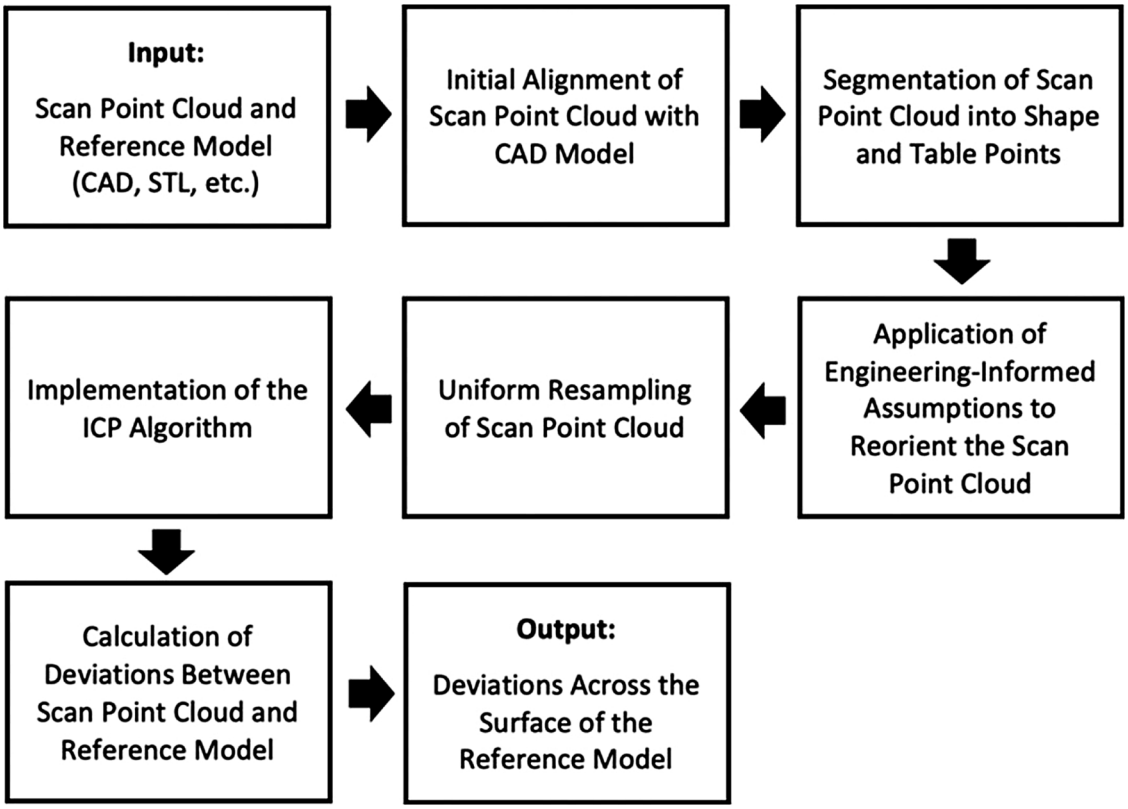

Fig. 4. Flowchart of the proposed procedure.

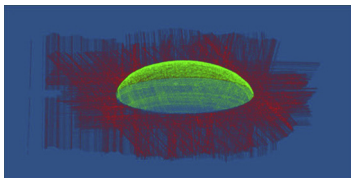

Fig. 5. Table points (red) and shape points (green). (For interpretation of the references to colour in this figure legend, the reader is referred to the web version of this article).

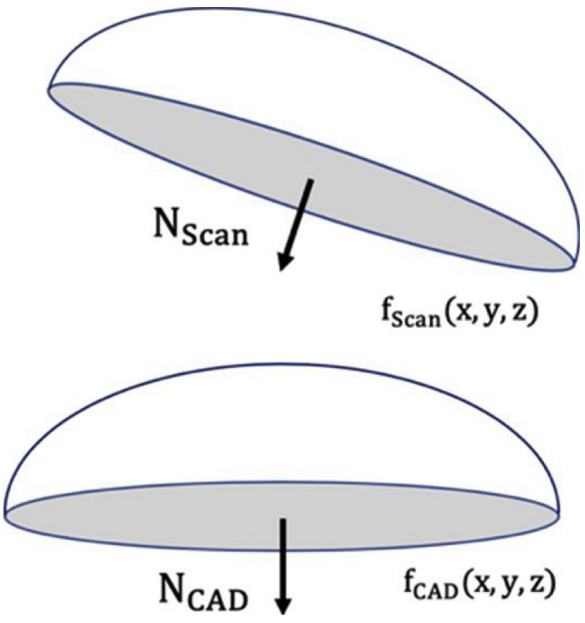

Fig. 6. Alignment of bottom plane of scan point cloud to CAD reference.

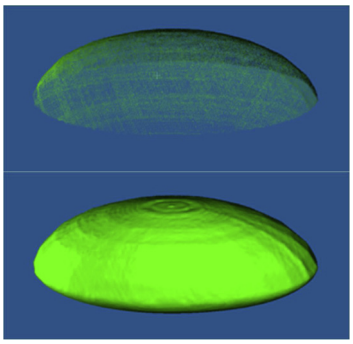

Fig. 7 and 8. Scan point cloud (top) and scan point cloud after screened Poisson surface reconstruction (bottom).

ICP algorithm. In order to ensure that the assumptions applied in Section 3.3 remain in effect, it is necessary to constrain the ICP algorithm to only perform translation along the x and y-axes, and rotation about the z-axis. In this way, the bottom planes of each shape will remain parallel and intersecting. As a result, the ICP algorithm will go from six degrees of freedom to three.

3.6. Deviation calculation

Once this registration is performed, deviations can be calculated as the distances from vertices on the CAD reference mesh to vertices on the scan point cloud. Results should be checked to ensure that they make intuitive sense.

4. Validation experiment

In this section, several of the registration issues discussed in Section 2 will be demonstrated quantitatively using simulated data. This will be

used to illustrate the potential magnitude of registration errors. Second, real data will be registered using unconstrained ICP, and the methodology presented in Section 2. The results produced by each of these techniques will be compared and discussed. All experiments were carried out using CloudCompare [38], open source software for manipulating and performing computations on point clouds and meshes, as well as MATLAB.

4.1. Demonstration of registration errors

The first set of experiments here seeks to demonstrate quantitatively the effects of the previously discussed errors using simulated data. Open source software An STL file of an egg-shaped part (80 mm x 40 mm x 20 mm) is first duplicated in order to create a reference design STL model, as well as a part into which error will be introduced. The second part is then modified in order to introduce a specific error. The initial alignment of these parts is considered ground truth, since their relative positions and orientations were not changed during the introduction of the dimensional errors. Intuitively, then, inspection of the differences between the two shapes would show precisely the errors that were introduced. After this, a point cloud is generated based on the modified STL. Finally, deviations are determined by measuring the distance from each vertex on the top surface of the design STL file to the point cloud, which simulates the result of a laser scan. Deviations are first calculated using the initial ground truth alignment. Then, registration of the scan point cloud to the mesh is performed using 50,000 sample points, and deviations are measured again. This allows the alignment errors introduced by the registration process to be evaluated.

The first error to be simulated is uneven point cloud density. Dimensional inaccuracy was introduced into the part by shrinking it along the x-axis by a factor of 5%. This results in the dimensional deviations shown on the left side of Fig. 9. In the following figures, surfaces that are blue correspond to dimensions that are too small, while red corresponds with dimensions that are too large. The top surface of each part is shown in the figures. The green axis in the bottom left corner of each figure corresponds to the positive y-axis, while the red corresponds to the positive x-axis. The positive z-axis comes out of the page. The right half of the part's corresponding point cloud was generated using 300,000 points, while the left half was generated using 100,000 points. After applying unconstrained ICP registration, the scanned point cloud is shifted 0.318 mm along the x-axis. Thus, while the average magnitude of deviations remains similar, their location changes. The deviations measured using each alignment as well as the extent of the introduced alignment error are given in Table 1. The affine transformation matrix describing the change in alignment produced by ICP registration is (mm):

$$\mathbf{T} = \begin{bmatrix} 1 & 0 & 0.003 & 0.318 \\ 0 & 1 & 0 & -0.006 \\ -0.003 & 0 & 1 & 0.116 \\ 0 & 0 & 0 & 1 \end{bmatrix}$$

The second error to be simulated is improper calibration along the z-axis, meaning that the height of the part is 5% too small. While the bottom layers of the part print with reasonable accuracy, each subsequent layer increases the absolute dimensional accuracy of the layer above it. In the first case, illustrated in Fig. 10, the scanned point cloud of this part has no bottom. In the second case, illustrated in Fig. 11, the scan includes the bottom of the hypothetical measured part. After applying unconstrained ICP registration for the first case, the scanned point cloud is shifted 0.690 mm along the z-axis. For the second case, the scanned point cloud is shifted 0.288 mm along the z-axis.

It can be seen that in both cases, registration moves the part upwards, reducing the magnitude of the deviations detected across the surface of the part. In the case where the point cloud includes bottom points, the magnitude of this shift is substantially smaller. One noteworthy observation is that in the first case, registration moves the scan point cloud so far upwards that negative deviations are turned into positive deviations around the bottom edges. This magnitude shift can present an especially difficult challenge for efforts to predict and model dimensional accuracy (Tables 2 and 3).

4.2. Evaluation of proposed registration methodology

A second experiment was then carried out to evaluate the impact of the changes to ICP introduced by the proposed registration methodology. The objective was to determine whether the proposed methodology generates deviation values that differ from those produced by ICP in statistically significant sense. In this experiment, four different shapes were printed on a fifth generation MakerBot Replicator FDM 3D printer. These shapes are shown in Fig. 12. Each shape was scanned three times using a Romer Arm 73 Series 7325 manufactured by Hexagon Manufacturing Systems with an accuracy of ± 80 μm. For

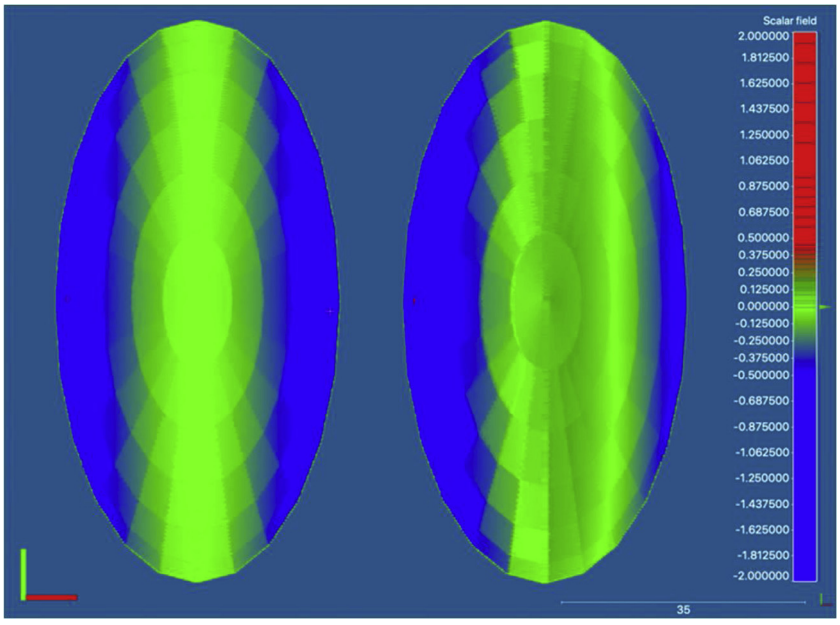

Fig. 9. Point cloud with uneven density: deformed part deviations before registration (left) and after registration (right).

Table 1
Comparison of measured deviations before and after registration.

	Before Registration	After Registration
Average Magnitude of Deviation for Vertices on STL (mm)	0.380	0.363
Average Deviation for Vertices on STL (mm)	0.378	0.308
RMSE from Registration (mm)	0.226	

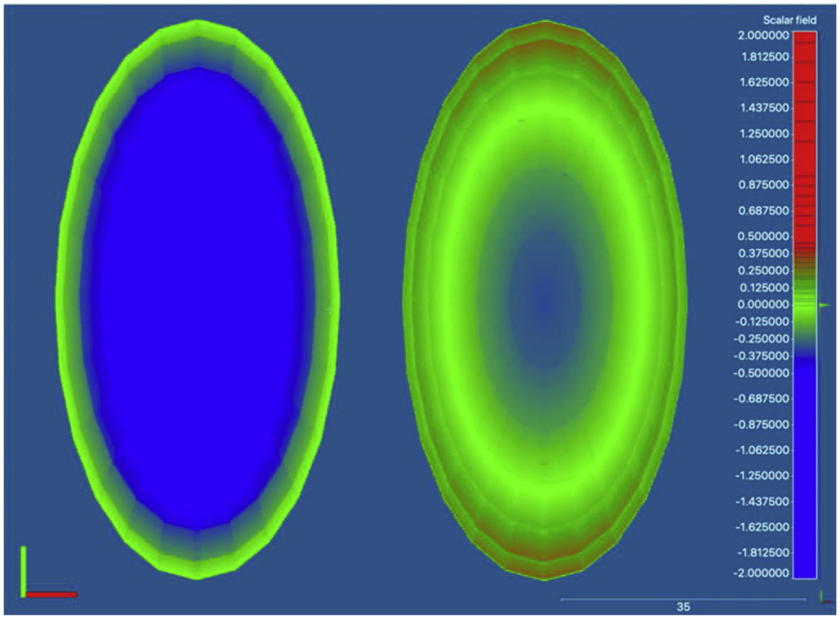

Fig. 10. Point cloud without bottom: deformed part deviations before registration (left) and after registration (right).

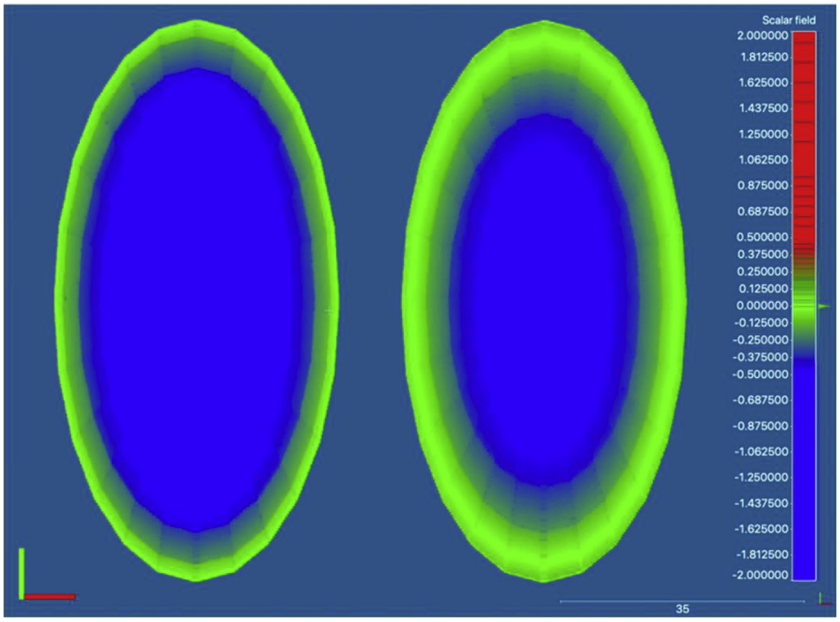

Fig. 11. Complete point cloud: deformed part deviations before registration (left) and after registration (right).

Table 2
Comparison of measured deviations before and after registration.

	Before Registration	After Registration
Average Magnitude of Deviation for Vertices on STL (mm)	0.401	0.141
Average Deviation for Vertices on STL (mm)	0.401	−0.036
RMSE from Registration (mm)	0.471	

Table 3
Comparison of measured deviations before and after registration.

	Before Registration	After Registration
Average Magnitude of Deviation for Vertices on STL (mm)	0.402	0.240
Average Deviation for Vertices on STL (mm)	0.401	0.219
RMSE from Registration (mm)	0.197	

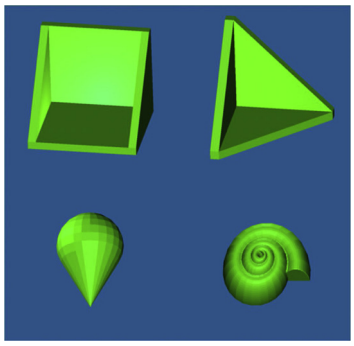

Fig. 12. CAD models of the parts used in the experiment.

each scan, three different users produced alignments using both unconstrained ICP and the proposed method.

Because the parts are printed with randomly generated errors from the manufacturing process, there are no ground truth deviation values to compare registration outcomes against. Instead, the RMS magnitude of deviations measured at each vertex on a given part's STL file will be determined and treated as the response variable. The method used is treated as a fixed effect with two levels: ICP and the proposed procedure. The shape of the object being evaluated is considered a random effect because of the infinite shape variety in practice. Four different shapes were chosen to incorporate a variety of common features, including both smooth geometries and sharp edges. It is important to evaluate the effect due to shape since this can strongly impact how different methods perform. Nested under the shapes is the scan factor, a random effect representing the scan-to-scan variation. Different scans may affect the relative density of the point cloud, as well as the orientation the part begins in before initial alignment. These effects were discussed in Section 2. Finally, the user producing alignment is also treated as a random effect. This accounts for patterns as well as varying quality in initial alignments. It is desirable for a registration method to be invariant to user, as this would mean that the method produces repeatable results. In this experiment, a given shape is considered to be a unit. This experimental design is illustrated in Fig. 13. A linear mixed effects model with nested random effects will be used to evaluate whether unconstrained ICP and the proposed method produce measurements of global error that differ in a significant way when tested on real manufacturing data. The proposed model is given as:

$$\mathscr{y} = \eta + \tau_i + \alpha_j + \beta_k + \gamma_{e(k)} + (\tau\gamma)_{il(k)} + (\tau\alpha)_{ij} + (\alpha\gamma)_{jl(k)} + \varepsilon_{ijkl}$$

where τ_i is the treatment effect from the method used, α_j is the random effect from user, β_k is the random effect due to shape, and $\gamma_{e(k)}$ is the random effect from scan, which is nested under the effect due to shape. Three potential interaction effects are also included in the model: $(\tau\gamma)_{il(k)}$, $(\tau\alpha)_{ij}$, and $(\alpha\gamma)_{jl(k)}$. The interaction between method and scan is included as different scans of the same object will likely interact differently with the ICP method, and potentially the proposed method. The interaction between method and user is included due to potential impact from the user's initial alignments on final results. Such an impact is undesirable. Finally, interactions between user and scan are accounted for in the model.

Before the proposed model is evaluated, it is helpful to look at one instance of alignments in depth for a single part and scan. It can be seen in Fig. 14 that unconstrained registration pulls the scan point cloud farther upwards than the proposed registration method. The scanned point cloud is shifted -0.046 mm along the x-axis, -0.019 mm along the y-axis and 0.128 mm along the z-axis. This results in a reduction in average magnitude of deviations by more than 10 %. Further, sections of the top surface of the part are considered too large as a result of this shift. This conforms well with the prediction that ICP will underestimate deviations that was presented in Section 2.2. A comparison of the measured deviations produced by the two different methods is given in Table 4. The affine transformation matrix describing the change in alignment produced by ICP registration is (mm):

$$\mathbf{T} = \begin{bmatrix} 1 & 0.002 & 0.001 & -0.046 \\ -0.002 & 1 & 0.001 & -0.019 \\ -0.001 & -0.001 & 1 & 0.128 \\ 0 & 0 & 0 & 1 \end{bmatrix}$$

The linear mixed-effects model was fit using the lme4 package in R via restricted maximum likelihood estimation (REML) [55]. REML is a popular form of maximum likelihood estimation for fitting linear mixed-effects models [56]. One advantage of this method over maximum likelihood estimation is that it produces unbiased estimates of variance parameters. After the proposed model was fit, terms representing statistically insignificant effects were systematically removed using backwards elimination until only statistically significant effects remained. This resulted in the following simplified model:

$$\mathscr{y} = \eta + \tau_i + \beta_k + (\tau\gamma)_{il(k)} + \varepsilon_{ijkl}$$

Which yields the analysis given in Tables 5 and 6. The random effects due to both user and scan were not found to be significant. As a result, the proposed method was not shown to be sensitive to operator changes. This is a necessary condition for a registration methodology, as it must produce repeatable results between operators. Interestingly, while the effect of scan variation itself wasn't shown to be significant in this model, the interaction between the method used and scans did prove to be significant. This makes intuitive sense in light of Section 2.1.

It can be seen in the fixed effect table that there is a statistically significant difference between the RMS of deviations produced by each of the methods. The proposed method tends to generate deviations of a greater magnitude. This is consistent with the tendency of unconstrained ICP to minimize deviations, which was demonstrated in Section 4.1. As a result, the experiment provides positive support for the hypothesis that the proposed method is less likely to underestimate geometric deviations.

5. Conclusion

In conclusion, several potential challenges for obtaining quality alignments of scan point clouds using ICP registration were discussed. These challenges were then illustrated using simulated data, which allowed for quantification of their impact on the accuracy of deviation measurements. The impact of each of these registration issues was shown to be significant enough to noticeably impact the measured deviations using simulated data.

A method to address some of these challenges based on engineering informed assumptions was presented. This method was used on real scan point cloud data, and compared to unconstrained ICP registration

		User 1: α_1		User 2: α_2		User 3: α_3	
		Method:		Method:		Method:	
		τ_1	τ_2	τ_1	τ_2	τ_1	τ_2
Shape 1: β_1 Scan:	1: $\gamma_{1(1)}$	0.167	0.243	0.168	0.243	0.167	0.241
	2: $\gamma_{2(1)}$	0.183	0.244	0.184	0.245	0.184	0.242
	3: $\gamma_{3(1)}$	0.184	0.250	0.194	0.249	0.185	0.250
Shape 2: β_2 Scan:	1: $\gamma_{4(2)}$	0.133	0.172	0.132	0.167	0.132	0.170
	2: $\gamma_{5(2)}$	0.127	0.160	0.131	0.165	0.127	0.158
	3: $\gamma_{6(2)}$	0.123	0.166	0.123	0.165	0.123	0.166
Shape 3: β_3 Scan:	1: $\gamma_{7(3)}$	0.124	0.133	0.123	0.134	0.123	0.133
	2: $\gamma_{8(3)}$	0.107	0.115	0.106	0.114	0.106	0.114
	3: $\gamma_{9(3)}$	0.101	0.122	0.103	0.122	0.101	0.125
Shape 4: β_3 Scan:	1: $\gamma_{10(4)}$	0.673	0.702	0.672	0.701	0.673	0.699
	2: $\gamma_{11(4)}$	0.594	0.685	0.588	0.686	0.588	0.685
	3: $\gamma_{12(4)}$	0.670	0.650	0.670	0.646	0.669	0.652

Fig. 13. Illustration of the experimental design.

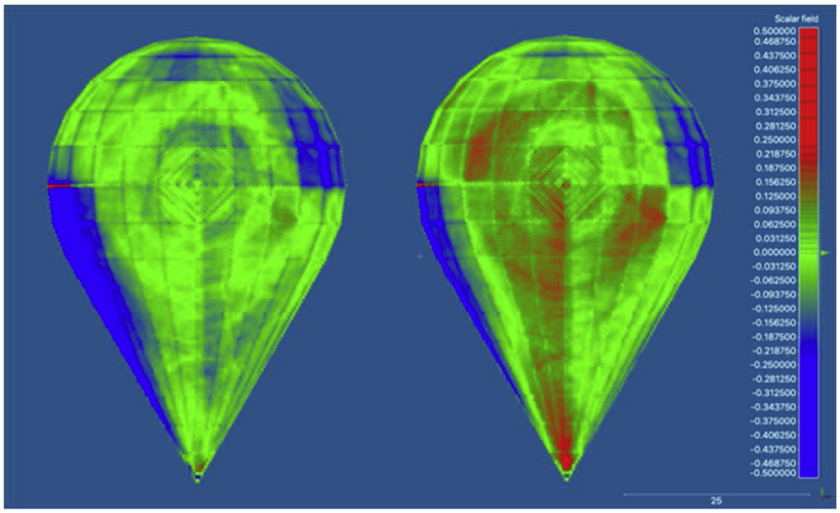

Fig. 14. Deviations using proposed method (left) and deviations using unconstrained ICP (right).

via a design of experiments approach. Differences between the magnitude of deviations produced by the alignments from each method were shown to be significant, while operator effects were not shown to be significant.

Declaration of Competing Interest

The authors declare that they have no known competing financial interests or personal relationships that could have appeared to influence the work reported in this paper.

Table 4
Comparison of measured deviations produced by unconstrained ICP and the proposed method.

	Unconstrained ICP	Proposed Method
Average Magnitude of Deviation for Vertices on STL (mm)	0.085	0.096
Average Deviation for Vertices on STL (mm)	0.017	0.089
RMS Difference Between Deviations for Each Method (mm)	0.092	

Table 5
Analysis of model fitting results for the fixed effect.

	Estimate	Std. Error	t Value	Pr(> |t|)
(Intercept)	0.265446	0.127317	2.085	0.128182
Proposed Method	0.037712	0.008713	4.329	0.000362

Table 6
Analysis of model fitting results for random effects.

	Std. Dev.	Pr(> Chisq)
Part (Intercept)	0.254336	< 2.2e-16
Method:Scan (Intercept)	0.021314	< 2.2e-16
Residual	0.001876	

Acknowledgements

The following work was supported by the National Science Foundation under grant CMMI-1901514, and by a graduate research fellowship from the Rose Hills Foundation. The authors wish to thank Austin Barrow and Mingdong Lyu for their efforts.

References

[1] Aboutaleb AM, Tschopp MA, Rao PK, Bian L. Multi-objective accelerated process optimization of part geometric accuracy in additive manufacturing. J Manuf Sci Eng 2017;139:101001https://doi.org/10.1115/1.4037319.
[2] Price S, Cheng B, Lydon J, Cooper K, Chou K. On process temperature in powder-bed electron beam additive manufacturing: process parameter effects. J Manuf Sci Eng 2014;136:061019https://doi.org/10.1115/1.4028485.
[3] Lanzotti A, Martorelli M, Staiano G. Understanding process parameter effects of RepRap open-source three-dimensional printers through a design of experiments approach. J Manuf Sci Eng 2015;137:011017https://doi.org/10.1115/1.4029045.
[4] Mohamed OA, Masood SH, Bhowmik JL. Optimization of fused deposition modeling process parameters: a review of current research and future prospects. Adv Manuf 2015;3:42–53. https://doi.org/10.1007/s40436-014-0097-7.
[5] Paul R, Anand S. Optimal part orientation in rapid manufacturing process for achieving geometric tolerances. J Manuf Syst 2011;30:214–22. https://doi.org/10.1016/j.jmsy.2011.07.010.
[6] Paul R, Anand S. Optimization of layered manufacturing process for reducing form errors with minimal support structures. J Manuf Syst 2015;36:231–43. https://doi.org/10.1016/j.jmsy.2014.06.014.
[7] Zhang B, Goel A, Ghalsasi O, Anand S. CAD-based design and pre-processing tools for additive manufacturing. J Manuf Syst 2019;52:227–41. https://doi.org/10.1016/j.jmsy.2019.03.005.
[8] Tong K, Joshi S, Lehtihet EA. Error compensation for fused deposition modeling (FDM) machine by correcting slice files. Rapid Prototyp J 2008;14:4–14. https://doi.org/10.1108/13552540810841517.
[9] Huang Q, Zhang J, Sabbaghi A, Dasgupta T. Optimal offline compensation of shape shrinkage for three-dimensional printing processes. IIE Trans (Institute Ind Eng) 2015;47:431–41. https://doi.org/10.1080/0740817X.2014.955599.
[10] Huang Q. An analytical foundation for optimal compensation of three-dimensional shape deformation in additive manufacturing. J Manuf Sci Eng 2016;138:061010https://doi.org/10.1115/1.4032220.
[11] Wang A, Song S, Huang Q, Tsung F. In-plane shape-deviation modeling and compensation for fused deposition modeling processes. IEEE Trans Autom Sci Eng 2017;14:968–76. https://doi.org/10.1109/TASE.2016.2544941.
[12] Cheng L, Wang A, Tsung F. A prediction and compensation scheme for in-plane shape deviation of additive manufacturing with information on process parameters. IISE Trans 2018;50:394–406. https://doi.org/10.1080/24725854.2017.1402224.
[13] Li Z, Liu X, Wen S, He P, Zhong K, Wei Q, et al. In situ 3D monitoring of geometric signatures in the powder-bed-fusion additive manufacturing process via vision sensing methods. Sensors (Switzerland) 2018;18. https://doi.org/10.3390/s18041180.
[14] Montazeri M, Rao P. Sensor-based build condition monitoring in laser powder bed fusion additive manufacturing process using a spectral graph theoretic approach. J Manuf Sci Eng 2018;140:091002https://doi.org/10.1115/1.4040264.
[15] Nuchitprasitchai S, Roggemann M, Pearce J. Three hundred and sixty degree Real-time monitoring of 3-D printing using computer analysis of Two camera views 1. 2017. https://doi.org/10.3390/jmmp1010002.
[16] Everton SK, Hirsch M, Stavroulakis PI, Leach RK, Clare AT. Review of in-situ process monitoring and in-situ metrology for metal additive manufacturing. Mater Des 2016;95:431–45. https://doi.org/10.1016/j.matdes.2016.01.099.
[17] Khanzadeh M, Chowdhury S, Marufuzzaman M, Tschopp MA, Bian L. Porosity prediction: supervised-learning of thermal history for direct laser deposition. J Manuf Syst 2018;47:69–82. https://doi.org/10.1016/j.jmsy.2018.04.001.
[18] Jafari-Marandi R, Khanzadeh M, Tian W, Smith B, Bian L. From in-situ monitoring toward high-throughput process control: cost-driven decision-making framework for laser-based additive manufacturing. J Manuf Syst 2019;51:29–41. https://doi.org/10.1016/j.jmsy.2019.02.005.
[19] Mitchell WF, Lang DC, Merdes TA, Reutzel EW, Welsh GS. Dimensional accuracy of titanium direct metal laser sintered parts. Solid Free Fabr Symp – An Addit Manuf Conf 2016:2029–42.
[20] Du Plessis A, Le Roux SG, Steyn F. X-ray computed tomography of consumer-grade 3D-printed parts. 3D Print Addit Manuf 2015;2:191–5. https://doi.org/10.1089/3dp.2015.0015.
[21] Decker N, Yee A. Assessing the use of binary blends of acrylonitrile butadiene styrene and post-consumer high density polyethylene in fused filament fabrication. Int J Addit Subtractive Mater Manuf 2017;1:161. https://doi.org/10.1504/IJASMM.2017.088203.
[22] Babu M, Franciosa P, Ceglarek D. Spatio-temporal adaptive sampling for effective coverage measurement planning during quality inspection of free form surfaces using robotic 3D optical scanner. J Manuf Syst 2019;53:93–108. https://doi.org/10.1016/j.jmsy.2019.08.003.
[23] Boehnen C, Flynn P. Accuracy of 3D scanning technologies in a face scanning scenario. Proc Int Conf 3-D Digit Imaging Model 3DIM 2005:310–7. https://doi.org/10.1109/3DIM.2005.13.
[24] Zhang Li, Curless B, Seitz S. Rapid shape acquisition using color structured light and multi-pass dynamic programming. Proceedings. First Int. Symp. 3D Data Process 2002. p. 24–36. https://doi.org/10.1109/TDPVT.2002.1024035.
[25] Flugge J, Wendt K, Danzebrink H, Abou-zeid A. Optical methods for dimensional metrology in production engineering. CIRP Ann Manuf Technol 2002;51:685–99.
[26] Harding K, editor. Handbook of optical dimensional metrology CRC Press; 2016. https://doi.org/10.1201/b13855.
[27] Stavroulakis PI, Leach RK. Invited review article: review of post-process optical form metrology for industrial-grade metal additive manufactured parts. Rev Sci Instrum 2016;87. https://doi.org/10.1063/1.4944983.
[28] Li Y, Gu P. Automatic localization and comparison for free-form surface inspection. J Manuf Syst 2006;25:251–68. https://doi.org/10.1016/S0278-6125(08)00007-1.
[29] Tam GKL, Cheng ZQ, Lai YK, Langbein FC, Liu Y, Marshall D, et al. Registration of 3d point clouds and meshes: a survey from rigid to nonrigid. IEEE Trans Vis Comput Graph 2013;19:1199–217. https://doi.org/10.1109/TVCG.2012.310.
[30] D. Girardeau-Montaut. Cloud Compare: Align n.d. https://www.cloudcompare.org/doc/wiki/index.php?title=Align (Accessed September 30, 2019).
[31] Aiger D, Mitra NJ, Cohen-Or D. 4-points congruent sets for robust pairwise surface registration. SIGGRAPH'08 Int Conf Comput Graph Interact Tech ACM SIGGRAPH 2008 Pap 2008 2008. https://doi.org/10.1145/1399504.1360684.
[32] Smith BK, Bian L, Rao P, Jafari-Marandi R, Tschopp MA, Khanzadeh M. Quantifying geometric accuracy with unsupervised machine learning: using self-organizing map on fused filament fabrication additive manufacturing parts. J Manuf Sci Eng 2017;140:031011https://doi.org/10.1115/1.4038598.
[33] Zhang R, Li H, Liu L, Wu M. A G-Super4PCS registration method for photogrammetric and TLS data in geology. ISPRS Int J Geo-Information 2017;6. https://doi.org/10.3390/ijgi6050129.
[34] Huang J, Kwok TH, Zhou C. V4PCS: volumetric 4pcs algorithm for global registration. Proc ASME Des Eng Tech Conf 2017;1:1–10. https://doi.org/10.1115/DETC2017-67452.
[35] Mellado N, Aiger D, Mitra NJ. SUPER 4PCS fast global pointcloud registration via smart indexing. Eurographics Symp Geom Process 2014;33:205–15. https://doi.org/10.1111/cgf.12446.
[36] Besl PJ, McKay ND. A method for registration of 3-D shapes. IEEE Trans Pattern Anal Mach Intell 14. 1992. p. 239–56. https://doi.org/10.1109/34.121791.
[37] Klar V, Pere J, Turpeinen T, Kärki P, Orelma H, Kuosmanen P. Shape fidelity and structure of 3D printed high consistency nanocellulose. Sci Rep 2019;9:1–13. https://doi.org/10.1038/s41598-019-40469-x.
[38] D. Girardeau-Montaut. CloudCompare n.d. https://www.cloudcompare.org (Accessed September 30, 2019).
[39] Alharbi N, Osman R, Wismeijer D. Factors influencing the dimensional accuracy of 3D-printed full-coverage dental restorations using stereolithography technology. Int J Prosthodont 2016;29:503–10. https://doi.org/10.11607/ijp.4835.
[40] Gelfand N, Ikemoto L, Rusinkiewicz S, Levoy M. Geometrically stable sampling for

the ICP algorithm. Proc Int Conf 3-D Digit Imaging Model 3DIM 2003 2003:260–7. https://doi.org/10.1109/IM.2003.1240258. Janua.
[41] Kwok T, Tang K. Improvements to the iterative closest point algorithm for shape registration in manufacturing. J Manuf Sci Eng 2016;138:011014https://doi.org/10.1115/1.4031335.
[42] Yu Y, Da F, Guo Y. Sparse ICP with resampling and denoising for 3D face verification. IEEE Trans Inf Forensics Secur 2019;14:1917–27. https://doi.org/10.1109/TIFS.2018.2889255.
[43] Chetverikov D, Svirko D, Stepanov D, Krsek P. The trimmed iterative closest point algorithm. Proc - Int Conf Pattern Recognit 2002;16:545–8. https://doi.org/10.1109/icpr.2002.1047997.
[44] Chetverikov D, Stepanov D, Krsek P. Robust Euclidean alignment of 3D point sets: the trimmed iterative closest point algorithm. Image Vis Comput 2005;23:299–309. https://doi.org/10.1016/j.imavis.2004.05.007.
[45] Dong J, Peng Y, Ying S, LieTrICP Hu Z. An improvement of trimmed iterative closest point algorithm. Neurocomputing 2014;140:67–76. https://doi.org/10.1016/j.neucom.2014.03.035.
[46] Minguez J, Montesano L, Lamiraux F. Metric-based iterative closest point scan matching for sensor displacement estimation. IEEE Trans Robot 2006;22:1047–54. https://doi.org/10.1109/TRO.2006.878961.
[47] Armesto L, Minguez J, Montesano L. A generalization of the metric-based iterative closest point technique for 3D scan matching. Proc - IEEE Int Conf Robot Autom 2010:1367–72. https://doi.org/10.1109/ROBOT.2010.5509371.
[48] Kapoutsis CA, Vavoulidis CP, Pitas I. Morphological iterative closest point algorithm. Lect Notes Comput Sci (Including Subser Lect Notes Artif Intell Lect Notes Bioinformatics) 1997;1296:416–23. https://doi.org/10.1007/3-540-63460-6_145.
[49] Kapoutsis CA, Vavoulidis CP, Pitas I. Morphological techniques in the iterative closet point algorithm. IEEE Int Conf Image Process 1998;1:808–12. https://doi.org/10.1109/icip.1998.723633.
[50] Yang J, Li H, Campbell D, Jia Y. Go-ICP: a globally optimal solution to 3D ICP point-set registration. IEEE Trans Pattern Anal Mach Intell 2016;38:2241–54. https://doi.org/10.1109/TPAMI.2015.2513405.
[51] Decker N, Huang Q. Geometric accuracy prediction for additive manufacturing through machine learning of triangular mesh data. Proc. ASME 2019 14th Int. Manuf. Sci. Eng. Conf. 2019. p. 1–9.
[52] Zhang W, Qi J, Wan P, Wang H, Xie D, Wang X, et al. An easy-to-use airborne LiDAR data filtering method based on cloth simulation. Remote Sens 2016;8:1–22. https://doi.org/10.3390/rs8060501.
[53] Möller T, Hughes JF. Efficiently building a matrix to rotate one vector to another. J Graph Tools 1999;4:1–4. https://doi.org/10.1080/10867651.1999.10487509.
[54] Kazhdan M, Hoppe H. Screened poisson surface reconstruction. ACM Trans Graph 2013;32:1–13. https://doi.org/10.1145/2487228.2487237.
[55] Bates D, Mächler M, Bolker B, Walker S. Fitting linear mixed-effects models using lme4. J Stat Softw 2015;67:201–10. https://doi.org/10.18637/jss.v067.i01.
[56] Bartlett MS. Properties of sufficiency and statistical tests. Proc R Soc London Ser A - Math Phys Sci 1937;160:268–82. https://doi.org/10.1098/rspa.1937.0109.